ELSEVIER

Ceramics International 32 (2006) 883–890

CERAMICS INTERNATIONAL

www.elsevier.com/locate/ceramint

In situ reaction synthesis and characterization of $Ti_3Si(Al)C_2$/SiC composites

D.T. Wan [a,b], Y.C. Zhou [a,*], Y.W. Bao [a], C.K. Yan [a]

[a] *Shenyang National Laboratory for Materials Science, Institute of Metal Research, Chinese Academy of Sciences, 72 Wenhua Road, Shenyang 110016, PR China*

[b] *Graduate School of Chinese Academy of Sciences, Beijing 100039, PR China*

Received 15 April 2005; received in revised form 21 May 2005; accepted 3 July 2005
Available online 12 September 2005

Abstract

The reaction route, microstructure, and properties of $Ti_3Si(Al)C_2$/SiC composites with 5–30 vol.% SiC content prepared by in situ hot pressing/solid–liquid reaction synthesis process are investigated. In contrast to monolithic $Ti_3Si(Al)C_2$, the SiC particle-reinforced composites exhibit higher elastic modulus, Vickers hardness, fracture toughness, improved wear, and oxidation resistance, but have a slight loss in flexural strength. The improvement in the properties is mainly ascribed to the contribution of SiC particles, and the strength degradation is due to the residual tensile stresses in the matrix.

Keywords: $Ti_3Si(Al)C_2$/SiC composites; Hardness; Wear behavior; Oxidation resistance

1. Introduction

Ti_3SiC_2 is a layered ternary carbide that possesses unique properties combining excellent characteristics of metals and ceramics such as low density, high strength and modulus, damage tolerance at room temperature, good machinability, and good resistance to thermal shock and oxidation below 1100 °C [1–6]. However, the low hardness (Vickers hardness of 4 GPa) and unsatisfied oxidation resistance above 1100 °C limit the application of Ti_3SiC_2 as high-temperature structural components. Previous study investigating on the electronic structure disclosed that low hardness originated from weak bonding between the Ti–C–Ti–C–Ti covalent bond chain and the Si atomic layer [7], which resulted in low shear modulus C_{44} [8]. Poor oxidation resistance above 1100 °C was caused by lack of continuous SiO_2 layer on the subsurface of the oxidized sample [9–11]. We have shown that the oxidation resistance can be improved by increasing the silicon content in the material [12] whereas hardness enhancement can be realized by particulate strengthening [13–15]. To achieve these goals, SiC particles were incorporated into a Ti_3SiC_2 matrix to fabricate Ti_3SiC_2/SiC composites. SiC was selected because it is hard, resistant to high temperature oxidation and creep, and thermodynamically stable with Ti_3SiC_2 [16]. In addition, the increased silicon content brought by the incorporated SiC particles was beneficial to the oxidation resistance of Ti_3SiC_2. It is thus expected that Ti_3SiC_2/SiC composites will exhibit improved hardness, wear, and oxidation resistance.

Due to these expected salient properties, a number of studies dealing with Ti_3SiC_2/SiC composites have been carried out. Tong et al. [2] fabricated a Ti_3SiC_2/20 vol.% SiC composite and studied its high-temperature mechanical properties. Li et al. [17] and Radhakrishnan et al. [18] synthesized a Ti_3SiC_2/14.2 vol.% SiC composite using displacement reactions to improve the mechanical properties of Ti_3SiC_2. Ho-Duc et al. [19] fabricated a Ti_3SiC_2/30 vol.% SiC composite by hot isostatic pressing (HIP) method. They found that hardness increased but strength was reduced compared to monolithic Ti_3SiC_2. It is worth noting that the Ti_3SiC_2/SiC composites fabricated by these methods always

* Corresponding author. Tel.: +86 24 23971765; fax: +86 24 23891320.
E-mail address: yczhou@imr.ac.cn (Y.C. Zhou).

0272-8842/$30.00
doi:10.1016/j.ceramint.2005.07.004

contain TiC and/or $TiSi_2$ impurities. We know that TiC is advantageous for enhancement of hardness and strength but deleterious to high-temperature oxidation resistance of Ti_3SiC_2-based materials [9,10]. The ill effects of TiC on oxidation resistance can be eliminated by substitution of Si with Al to form $Ti_3(Si_{1-x}Al_x)C_2$ solid solutions because Al is favorable in the formation of $Ti_3Si(Al)C_2$ and is effective in removing the TiC impurity from Ti_3SiC_2 [20,21]. To understand the effects of SiC on the mechanical properties and oxidation behavior of Ti_3SiC_2 better, we use TiC free $Ti_3Si(Al)C_2$ as the matrix for $Ti_3Si(Al)C_2$/SiC composites in this study. In the present paper, we describe the synthesis, microstructure, mechanical properties, and oxidation behaviors of $Ti_3Si(Al)C_2$/SiC composites. The main contributions of this work are: (1) bulk $Ti_3Si(Al)C_2$/SiC composites were in situ synthesized at relatively low temperatures; (2) no impurity phase like TiC co-exists with SiC; and (3) the effects of SiC on the microstructure and properties of the $Ti_3Si(Al)C_2$/SiC composites can be well understood.

2. Experimental

2.1. Material preparation

Previous studies [22,23] demonstrated that Ti_3SiC_2 and SiC could simultaneously be formed from elemental powders of Ti, Si, and graphite at relatively low temperatures, which indicated that Ti_3SiC_2/SiC composites could be synthesized in situ. Thus, we used elemental powders of Ti (99%, 300 mesh), Si (99%, 400 mesh), graphite (98%, 200 mesh), and Al (99.5%, 200 mesh) as initial materials. Al was added to eliminate TiC and to form a $Ti_3Si_{0.95}Al_{0.05}C_2$ matrix. The contents of SiC in $Ti_3Si(Al)C_2$/SiC composites were adjusted by controlling the amounts of Si and graphite. Table 1 lists the target compositions of $Ti_3Si(Al)C_2$ and $Ti_3Si(Al)C_2$/SiC composites with different amounts of SiC. The SiC contents in the final bulk composites determined by X-ray diffraction were also depicted and compared in Table 1. Bulk $Ti_3Si(Al)C_2$ and $Ti_3Si(Al)C_2$/SiC composites were prepared by in situ hot pressing/solid–liquid reaction process [24], wherein both SiC and $Ti_3Si(Al)C_2$ matrices were synthesized in situ. In this process, elemental powders of Ti, Si, Al and graphite were precisely weighed according to the target compositions and mixed in a polyurethane mill for 15 h in a wet medium. After drying at room temperature, the mixtures were screened through a 60-mesh sieve and then were put in a ϕ 50 mm graphite mold coated with a layer of boron nitride (BN) and cold pressed. The green compacts were then hot pressed at 30 MPa under a flowing Ar atmosphere at 1560 °C for 60 min (this temperature is suitable to warrant the simultaneous formation of $Ti_3Si(Al)C_2$ and SiC), and subsequently annealed at 1400 °C for 30 min.

2.2. Characterization of $Ti_3Si(Al)C_2$/SiC composites

The densities of the as-prepared composites were determined by Archimedes method. The phase compositions were identified by X-ray diffraction using powders drilled from the bulk samples. The XRD data were collected by a step-scanning diffractometer with Cu Kα radiation (Rigaku D/max -2400, Japan). To determine the true SiC contents in the $Ti_3Si(Al)C_2$/SiC composites, quantitative phase analysis was conducted. The data used for quantitative analysis had an accuracy better than 0.02°. Two methods, i.e. the Internal Standard method [25] and the Rietveld method [26] were used to calculate the SiC contents. In the Internal Standard method, the mass fraction of SiC was calculated using the equation:

$$\frac{I_{SC}}{I_{TSC}} = K\frac{W_{SC}}{W_{TSC}} = K\frac{W_{SC}}{1 - W_{SC}} \quad (1)$$

where I_{SC} and I_{TSC} are the intensities of selected lines in the diffraction pattern of SiC and $Ti_3Si(Al)C_2$, respectively; W_{SC} and W_{TSC}, the mass fractions of SiC and $Ti_3Si(Al)C_2$ phase, respectively; K is a constant which depends on the nature of SiC and $Ti_3Si(Al)C_2$ as well as the geometry of the instrumentation, and can be calibrated using different weight ratios of SiC to $Ti_3Si(Al)C_2$ as mixtures. In the Rietveld method, crystal structure and peak profile parameters are refined in several stages. The complete profile of the powder diffraction pattern is refined by employing a DBWS code [27] in Cerius^2 computational program for materials research (Molecular Simulation Inc., USA). The intensity is represented by:

$$I_{\text{Rietveld}}(2\theta) = b(2\theta) + S\sum_K L_K|F_K|^2\phi(2\theta_i - 2\theta_K)P_K A_K \quad (2)$$

Table 1
The target SiC contents compared with those calculated by two different methods in $Ti_3Si(Al)C_2$/SiC composites

The target SiC contents in $Ti_3Si(Al)C_2$/SiC composites		The calculated SiC contents by the Internal Standard method		The calculated SiC contents by the Rietveld method	
vol.%	wt.%	vol.%	wt.%	vol.%	wt.%
0	0	1.2	0.9	4.1	3.0
5	3.6	6.9	5.0	9.4	6.9
10	7.4	9.6	7.1	11.9	8.8
20	15.2	18.9	14.3	18.7	14.1
30	23.5	31.4	24.6	29.2	22.8

where $b(2\theta)$ is the background intensity; S, scale factor; L_K, contains the Lorentz polarization and multiplicity factors; ϕ, profile function; P_K, preferred orientation function; A_K, absorption factor; and F_K, structure factor. The index K represents Miller indices for the Bragg reflections. In the Rietveld method, the mass fraction of a phase q, W_q, is given by [26,28]:

$$W_q = \frac{S_q M_q V_q}{\sum(S_i M_i V_i)} \quad (3)$$

where S is the Rietveld scale factor for the phase q; M, molar mass; and V, volume of the unit cell. The advantages of the Rietveld method include, viz. the calibration constants are computed rather than measured by experiments; all the peaks in the pattern play a part in the analysis; the use of a continuous fitting function provides a much improved background fit, and finally, the effects of preferred orientation and extinction are reduced.

The microstructure of the composites was examined in a S-360 scanning electron microscope (Cambridge Instruments Ltd., UK) equipped with an energy-dispersive spectroscopy (EDS) system. To expose the $Ti_3Si(Al)C_2$ and SiC grains, samples were mechanically polished and etched by an HNO_3:HF:H_2O (1:1:2) solution before SEM observation.

Vickers hardness was tested on the polished surfaces under various loads of 0.98, 1.96, 2.94, 4.90, and 9.80 N with a dwell time of 15 s. Three-point bending tests were performed to measure the flexural strength, elastic modulus, and fracture toughness. The specimens for elastic modulus and flexural strength tests were rectangular bars of 3 mm × 4 mm × 36 mm in size. The elastic modulus was obtained using the ratio of load increment to the deflection increment [29]. Single-edge notched beam (SENB) specimens with a size of 4 mm × 8 mm × 36 mm were used to measure the fracture toughness. The notch was made 4 mm in depth and ~0.15 mm in width. The crosshead speed was 0.5 mm min^{-1} for flexural strength and elastic modulus tests, and 0.05 mm min^{-1} for fracture toughness measurements.

Friction and wear tests were performed under nonlubrication conditions with point contact wear mode using a ball on a flat sliding block specimen. All wear tests were conducted with a reciprocating machine (UMT-2 Multi-Specimen Test System, CETR, USA) at room temperature with a relative humidity of 40–55%. The ball was 4 mm in diameter and made of 52,100 bearing steel. A load of 10 N was applied downward through the ball against the flat specimen mounted on a reciprocating drive. The total sliding distance was 30 m at a sliding velocity of 30 mm s^{-1} for 1000 s. Before and after tests, all the samples were ultrasonically cleaned, dried, and weighed. The wear coefficient (W) is given by:

$$W = \frac{\Delta m}{PL} \quad (4)$$

where Δm (kg) is the weight loss; P (N) is the applied load; and L (m) is the total sliding distance.

The isothermal oxidation kinetics of the $Ti_3Si(Al)C_2$-based composites were investigated at 1100 °C in air for 20 h and compared with that obtained from Ti_3SiC_2. Specimens with dimensions of 3 mm × 4 mm × 15 mm were ground to 1000 grit SiC, polished using diamond paste, chamfered and degreased in acetone. The samples were suspended with a Pt wire in a vertical Setsys16/18 thermal balance (SETARAM, France). The continuous mass gains were automatically recorded as a function of time.

3. Results

3.1. Synthesis, phase compositions, and microstructure

The reaction route for the synthesis of Ti_3SiC_2 from elemental powders of Ti, Si, and C, was investigated in many of the previous studies [22–24,30]. Briefly, intermediate phases such as Ti_5Si_3, TiC, $TiSi_2$, and SiC form during heating depending on the initial compositions of the powder mixture and temperature. Generally, Ti_3SiC_2 forms at 1400–1500 °C in Si-rich Ti, Si, and C powder mixtures according to the following reactions [31]:

$$Si(s) \rightarrow Si(l) \quad (5)$$

$$3Ti(s) + Si(l) + 2C(s) \xrightarrow{Si(l)} Ti_3SiC_2(s) \quad (6)$$

The impurity phase such as TiC can be eliminated by partial substitution of Si with Al [20,21]. Higher synthesis temperature (above 1500 °C) or surplus in C in the initial powder mixture favors the formation of SiC [22,30,31]. The reaction can be simply described as:

$$Si + C \rightarrow SiC \quad (7)$$

Based on these facts, we synthesized Ti_3SiC_2/SiC composites at 1560 °C utilizing extra Si and graphite to control the SiC content. In addition, 5 at.% of silicon in the Ti_3SiC_2 matrix was substituted with Al to make sure that no TiC existed in the final composites. Thus, the true composition of the matrix is $Ti_3Si_{0.95}Al_{0.05}C_2$ and is denoted as $Ti_3Si(Al)C_2$ hereafter for brevity.

Fig. 1 shows the X-ray diffraction patterns of $Ti_3Si(Al)C_2$/SiC composites with different amounts of SiC. The crystalline phases were identified as $Ti_3Si(Al)C_2$ and β-SiC. No peaks from impurity phases such as TiC and Ti_5Si_3 could be detected via XRD. The intensity ratios of β-SiC (1 1 1) ($I_{SC(111)}$) to $Ti_3Si(Al)C_2$ (1 0 4) ($I_{TSC(104)}$) increase with the increment of SiC contents. To determine the true SiC contents in $Ti_3Si(Al)C_2$/SiC composites, quantitative phase analysis was conducted using both the Internal Standard method and the Rietveld method. In the Internal Standard method, the constant K value of 1.46 was calibrated using the intensity ratios $I_{SC(111)}/I_{TSC(104)}$ versus the added β-SiC amount in a series of SiC–$Ti_3Si(Al)C_2$

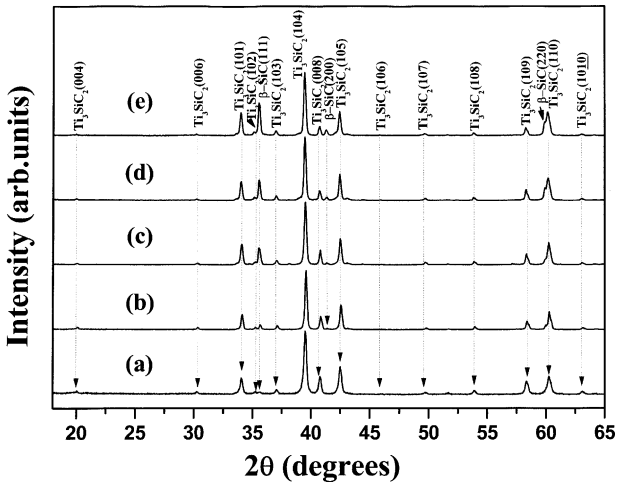

Fig. 1. X-ray diffraction patterns of $Ti_3Si(Al)C_2$/SiC composites with different SiC contents at 0 vol.% (a), 5 vol.% (b), 10 vol.% (c), 20 vol.% (d), and 30 vol.% (e). Note the absence of TiC impurity in all the composites.

powder mixtures. Then the relative SiC contents can be calculated by:

$$W_{SC} = \frac{I_{SC}/I_{TSC}}{1.46 + I_{SC}/I_{TSC}} \quad (8)$$

where $I_{SC(111)}$ and $I_{TSC(104)}$ used in Eq. (8) are the integrated intensities of β-SiC (1 1 1) at $2\theta = 35.60^\circ$ and $Ti_3Si(Al)C_2$ (1 0 4) at $2\theta = 39.58^\circ$, respectively. In the Rietveld method, the final reliability factors for the composites in the whole composition range are around 10, e.g. R-P = 9.78% and R-WP = 13.50% for $Ti_3Si(Al)C_2$, demonstrating the necessary accuracy of the refinement. Table 1 compares the target SiC contents with those determined from quantitative phase analysis using the two above-mentioned methods. It shows that these values are quite close especially for the composites with SiC over 5 vol.%. Thus, we use the target SiC contents instead of the true values for the $Ti_3Si(Al)C_2$/SiC composites hereafter.

The samples prepared by this process were fully dense (98–99% of the theoretical density). Fig. 2 compares the backscattered electron images of the etched surfaces of $Ti_3Si(Al)C_2$ (Fig. 2(a)), $Ti_3Si(Al)C_2$/10 vol.% SiC (Fig. 2(b)), $Ti_3Si(Al)C_2$/20 vol.% SiC (Fig. 2(c)), and $Ti_3Si(Al)C_2$/30 vol.% SiC (Fig. 2(d)) composites. In Fig. 2(a), the large elongated $Ti_3Si(Al)C_2$ grains show layered characteristics and their longitudinal edges are parallel to (0 0 0 1) planes of Ti_3SiC_2 [32]. Although the other grains seem small in size, they are also elongated grains with their longitudinal direction perpendicular or inclined to the surface. In Fig. 2(b)–(d), the large crystallites in the dark gray region are rich in Si but less in Ti by EDS and are identified as β-SiC. The grains in the light-gray region are composed of Ti, Si, Al, and C, which are recognized as $Ti_3Si(Al)C_2$ matrix. No TiC was found in SEM micrographs. The β-SiC platelets are uniformly dispersed in the $Ti_3Si(Al)C_2$ matrix. Moreover, the average sizes of grain $Ti_3Si(Al)C_2$ gradually reduces with increase of SiC contents. Table 2 compares the measured average size of grain of $Ti_3Si(Al)C_2$ and SiC in the composites. The data in the table reveal that grain growth of $Ti_3Si(Al)C_2$ is inhibited by the presence of SiC through a pinning mechanism [33].

3.2. Mechanical properties

Fig. 3(a) compares the Vickers hardness of the $Ti_3Si(Al)C_2$ matrix and the $Ti_3Si(Al)C_2$/30 vol.% SiC composite. Similar to Ti_3SiC_2, not only the measured Vickers hardness of $Ti_3Si(Al)C_2$ matrix and $Ti_3Si(Al)C_2$/30 vol.% SiC composite but also the scatter in the hardness data decrease with increasing load and reach a constant value at indentation loads over 4.9 N. Thus, we use the Vickers hardness data produced at an indentation load of 9.8 N to investigate the effect of SiC on the hardness. The results, as depicted in Fig. 3(b), indicate that the measured hardness linearly increases with increment of SiC content. As in Ti_3SiC_2 and Ti_3AlC_2 [4,34], no indentation-induced cracks are observed at the corners of the indent, which indicates that the $Ti_3Si(Al)C_2$/SiC composites are tolerant to surface damage. SEM observation on the morphology of the indents reveals that the grains in the composites are squeezed out from the indentation and piled up at the perimeter of the indent. Many grains have been broken into debris or delaminated under shear stress. The microstructure of the composites in regions far from the indent remained unchanged, viz. the damage was confined to surface indent which underpinned damage tolerance.

Change of the elastic modulus of $Ti_3Si(Al)C_2$/SiC composites versus SiC content is shown in Fig. 4. One can see that the elastic modulus linearly increases with SiC content and obeys the rule of mixture. The enhanced elastic modulus and Vickers hardness of the composites are mainly attributed to the introduction of increasingly higher elastic modulus (~440 GPa) and Vickers hardness (~25.5 GPa) of SiC into the $Ti_3Si(Al)C_2$ matrix. As predicted from the rule of mixture, the measured elastic modulus data fitted well with the calculated ones in the composition range.

Fig. 5 shows the flexural strength and fracture toughness of $Ti_3Si(Al)C_2$/SiC composites with different SiC contents, displaying different trends between them. The flexural strength dropped dramatically when the SiC content was 5 vol.%, and then declined slightly to 355 ± 10.3 MPa with increasing SiC content up to 30 vol.%; whereas the fracture toughness increased with increase of SiC content and reached a maximum value of 7.0 ± 0.27 MPa $m^{1/2}$ for $Ti_3Si(Al)C_2$/20 vol.% SiC, and then slightly decreased to 7.0 ± 0.33 MPa $m^{1/2}$ for $Ti_3Si(Al)C_2$/30 vol.% SiC.

3.3. Wear and oxidation resistance

The results in the previous section show that the hardness and elastic modulus of $Ti_3Si(Al)C_2$ are enhanced by

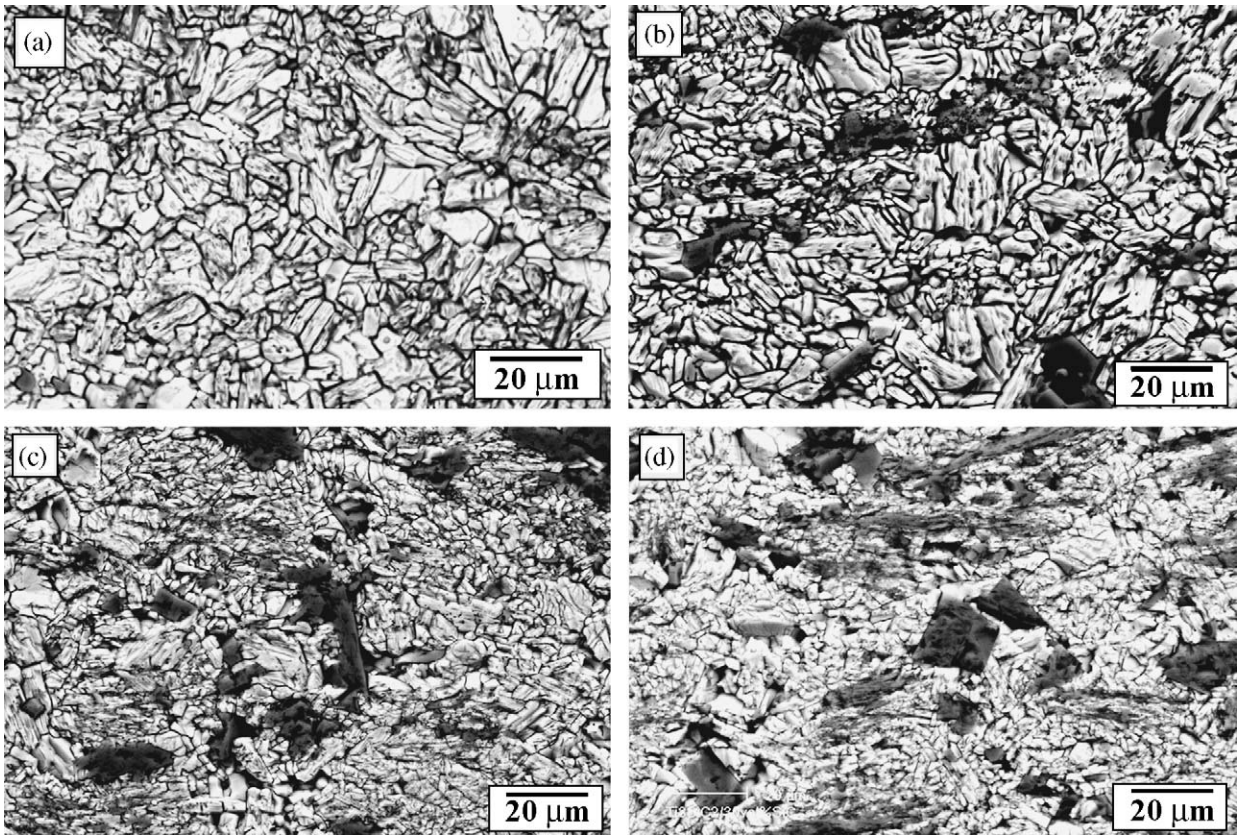

Fig. 2. Backscattered electron images of the etched surfaces of $Ti_3Si(Al)C_2$/SiC composites with SiC contents at 0 vol.% (a), 10 vol.% (b), 20 vol.% (c), and 30 vol.% (d). The light-gray phase is $Ti_3Si(Al)C_2$ matrix and the dark phase is SiC.

incorporation of SiC. It is thus expected that wear resistance would also be improved. Fig. 6 shows the friction coefficients of $Ti_3Si(Al)C_2$ and $Ti_3Si(Al)C_2$/SiC composites with different SiC content against 52,100 bearing steel ball which has a bulk hardness of HRC 59–62. The tests were carried out at a sliding velocity of 0.03 m s^{-1} under a constant load of 10 N and the total sliding distance was 30 m. It is noted that the friction coefficient of $Ti_3Si(Al)C_2$ is usually as low as 0.20 at the beginning of sliding and then reaches a stable value of 0.80–0.90. Whereas the composites with SiC contents over 5 vol.% displays a high friction coefficient at the contact period and then drops to low friction coefficients in the range of 0.35–0.50. Fig. 7 shows the variation of the wear coefficients as a function of SiC content. The wear coefficients decrease significantly with increase of SiC content, which means that the wear resistance can be greatly enhanced by adding SiC particles into $Ti_3Si(Al)C_2$. The strong hardness of SiC is the major factor in enhancing the wear resistance of $Ti_3Si(Al)C_2$.

The obtained results demonstrate that the $Ti_3Si(Al)C_2$/SiC composites possess superior mechanical and wear properties that project it as a promising structural material. Another important property for structural materials is oxidation resistance. Because both Si and Al content are greater than those in the monolithic Ti_3SiC_2, better oxidation resistance is expected. Fig. 8 shows the mass gain per unit area as a function of oxidation time for various $Ti_3Si(Al)C_2$/SiC composite samples oxidized at 1100 °C in air for 20 h. It was found that mass gain decreased with increment of SiC content, viz. the oxidation resistance increased with increase of SiC content. The improvement in oxidation resistance was attributed to the following facts. First, there was no TiC

Table 2
Measured average grain sizes of $Ti_3Si(Al)C_2$ and SiC grains varying with the SiC contents in the $Ti_3Si(Al)C_2$/SiC composites

Samples	Average grain size			
	$Ti_3Si(Al)C_2$		SiC	
	Grain length (μm)	Grain width (μm)	Grain length (μm)	Grain width (μm)
$Ti_2Si(Al)C_2$	16.1 ± 9.3	4.2 ± 1.4		
$Ti_3Si(Al)C_2$–10 vol.% SiC	12.8 ± 7.9	4.0 ± 1.8	16.2 ± 6.5	8.2 ± 3.1
$Ti_3Si(Al)C_2$–20 vol.% SiC	11.1 ± 6.5	3.9 ± 1.2	16.7 ± 9.9	8.7 ± 3.7
$Ti_3Si(Al)C_2$–30 vol.% SiC	10.9 ± 4.7	4.1 ± 1.3	17.3 ± 7.2	8.6 ± 2.9

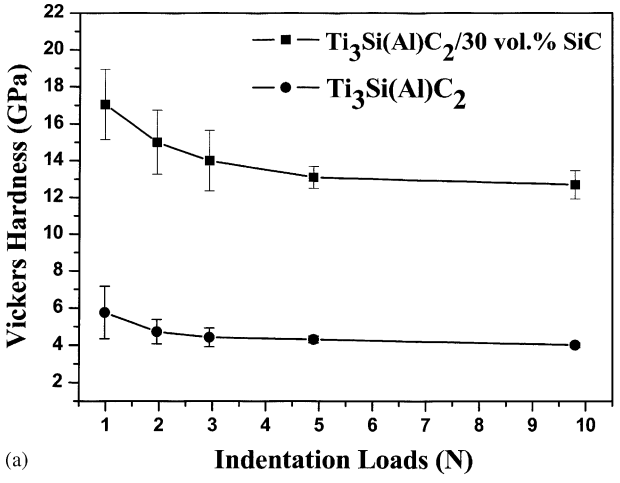

(a)

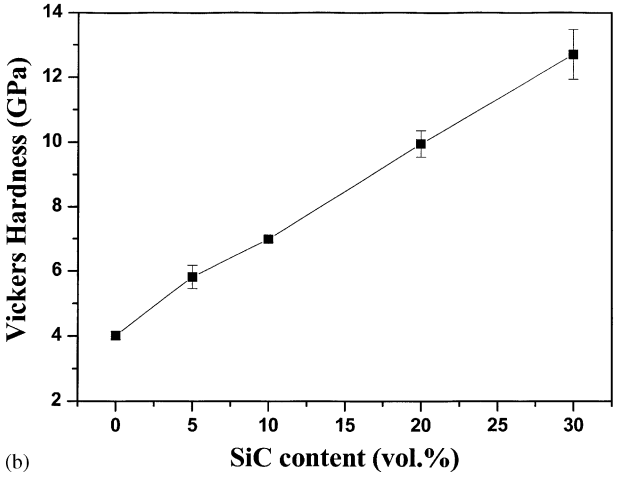

(b)

Fig. 3. (a) Vickers hardness of the monolithic $Ti_3Si(Al)C_2$ and $Ti_3Si(Al)C_2$/30 vol.% SiC composite as a function of indentation loads. (b) Vickers hardness vs. SiC contents in $Ti_3Si(Al)C_2$/SiC composites (at 9.8 N).

impurity phase in the composite. Second, $Ti_3Si_{0.95}Al_{0.05}C_2$ had better oxidation resistance than Ti_3SiC_2 [20]. Finally, SiC had excellent oxidation resistance at high temperatures

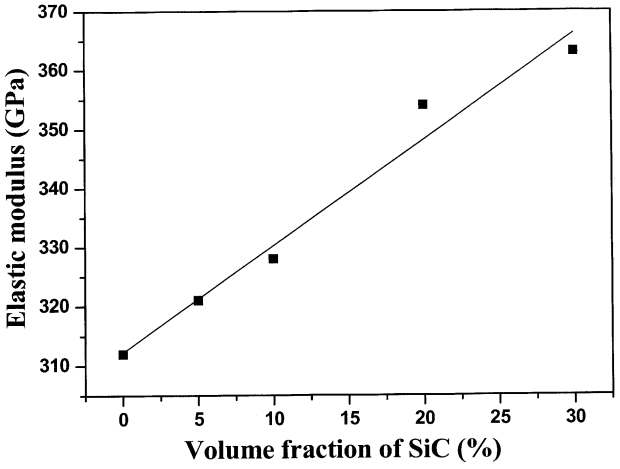

Fig. 4. Measured elastic modulus vs. SiC contents in $Ti_3Si(Al)C_2$/SiC composites.

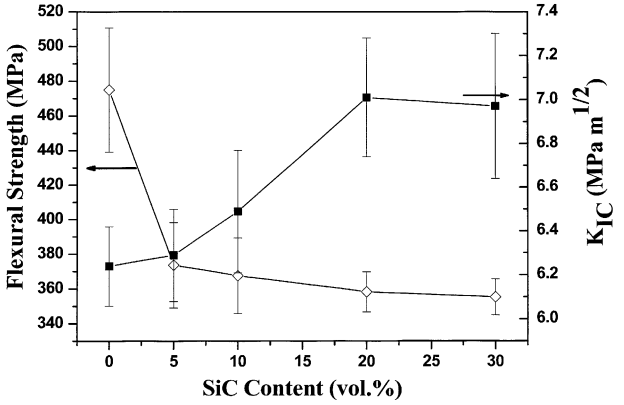

Fig. 5. Flexural strength and fracture toughness (K_{IC}) vs. SiC contents in $Ti_3Si(Al)C_2$/SiC composites.

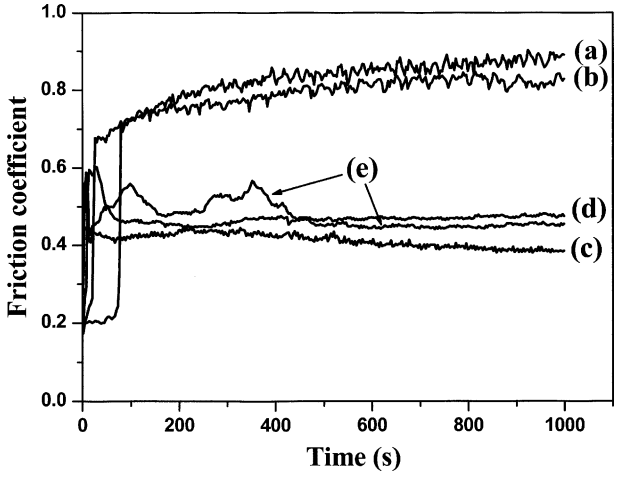

Fig. 6. Friction coefficients vs. sliding time of $Ti_3Si(Al)C_2$/SiC composites with different SiC content at 0 vol.% (a), 5 vol.% (b), 10 vol.% (c), 20 vol.% (d), and 30 vol.% (e) against 52,100 bearing steel ball in a nonlubrication reciprocation motion test.

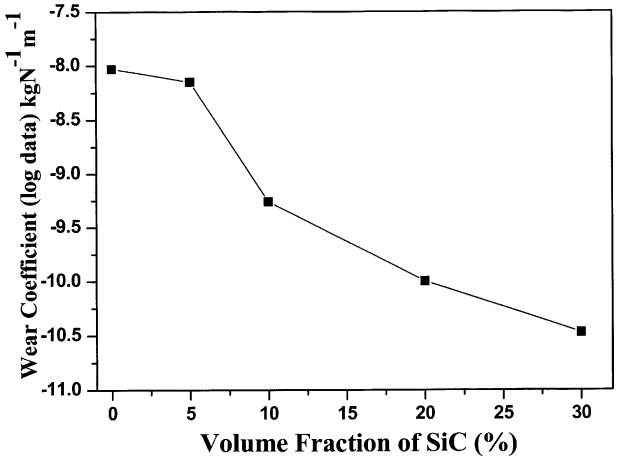

Fig. 7. Effect of the SiC contents on the wear coefficients of the composites against 52,100 bearing steel ball in a nonlubrication reciprocation motion test.

Table 3
Summary of the typical properties of monolithic $Ti_3Si(Al)C_2$, $Ti_3Si(Al)C_2$/10 vol.% SiC and $Ti_3Si(Al)C_2$/30 vol.% SiC composites

Properties	$Ti_3Si(Al)C_2$	$Ti_3Si(Al)C_2$/10 vol.% SiC	$Ti_3Si(Al)C_2$/30 vol.% SiC
Density (g/cm^3)	4.47	4.33	4.03
Elastic modulus (GPa)	312	328	363
H_v (GPa)	4.02	6.99	12.70
Flexural strength (MPa)	475.0	367.6	355.3
Fracture toughness (MPa m$^{1/2}$)	6.24	6.49	6.97
Wear coefficients (kg N^{-1} m^{-1})	9.41×10^{-9}	5.50×10^{-10}	3.36×10^{-11}
Parabolic rate constants at 1100 °C (kg^2 m^{-4} s^{-1})	2.9×10^{-8}	2.1×10^{-8}	9.8×10^{-9}

and the incorporation of SiC increased the Si content in the composites.

4. Discussion

Table 3 summarizes the typical properties of the monolithic $Ti_3Si(Al)C_2$, $Ti_3Si(Al)C_2$/10 vol.% SiC, and $Ti_3Si(Al)C_2$/30 vol.% SiC. The data in Table 3 show that $Ti_3Si(Al)C_2$/30 vol.% SiC composite has superior mechanical properties, wear, and oxidation resistance, but has a slight loss in the flexural strength. The decreased strength needs an investigation about the effect of SiC on the strength of the composites and will be discussed in this section.

The phenomenon that the room temperature flexural strengths of Ti_3SiC_2/30 vol.% SiC and Ti_3SiC_2/30 vol.% TiC composites were lower than that of the unreinforced Ti_3SiC_2 matrix was also reported by Ho-Duc et al. [19]. Here we consider the effect of reinforcing particles (SiC) on strength in two ways. Firstly, strengthening is expected due to the reduced grain sizes of the $Ti_3Si(Al)C_2$ matrix. However, the grain sizes of the in situ prepared reinforcing phase SiC are quite large, e.g. some grains are more than 50 μm in length and 5–10 μm in thickness, which are deleterious to strength like in the case of the coarse-grained Ti_3SiC_2 [6]. Secondly, because of the thermal mismatch between the reinforcement phase and the matrix, $\alpha_p < \alpha_m$ (α_p is 4.3×10^{-6} K^{-1} for SiC and α_m is 9.1×10^{-6} K^{-1} for $Ti_3Si(Al)C_2$), residual compressive stresses would occur in the radial direction and tensile stresses occur in the tangential direction (around SiC particles) during cooling. The thermally induced residual tensile stress on the matrix phase (as opposite to the reinforcement) weakened the strength of $Ti_3Si(Al)C_2$, thus the lower flexural strengths of the composites were measured. Note that the strength decreased severely only when SiC content was 5 vol.%, which indicates that increase of SiC content does not result in increase of the residual stresses that depend on temperature drop and the difference in thermal expansion between SiC and the matrix. Thus, the reduction in flexural strength is mainly due to the presence of residual tensile stresses in the matrix.

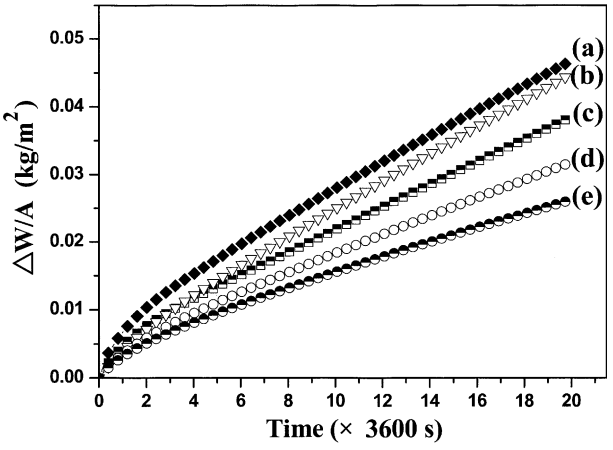

Fig. 8. Plots of mass gain per unit area vs. oxidation time for the $Ti_3Si(Al)C_2$/SiC samples with different SiC content at 0 vol.% (a), 5 vol.% (b), 10 vol.% (c), 20 vol.% (d), and 30 vol.% (e) oxidized at 1100 °C in air for 20 h.

5. Conclusions

Fully dense and TiC-free $Ti_3Si(Al)C_2$/SiC composites were synthesized by in situ hot pressing/solid–liquid reaction process under a pressure of 30 MPa in a flowing Ar atmosphere at 1560 °C for 60 min and 1400 °C for 30 min. Compared to monolithic $Ti_3Si(Al)C_2$, these SiC particle-reinforced composites exhibit higher elastic modulus, Vickers hardness, fracture toughness, improved wear and oxidation resistances, but a slight loss in flexural strength. $Ti_3Si(Al)C_2$/30 vol.% SiC composite shows the highest elastic modulus (16% higher than that of $Ti_3Si(Al)C_2$), hardness (217% higher), wear resistance (the wear coefficient decreases by about 2 orders of magnitude), oxidation resistance (the parabolic rate constant at 1100 °C decreases by about 1 order of magnitude), and fracture toughness (11.7% higher), whereas the flexural strength is about 25% lower than that of $Ti_3Si(Al)C_2$. The improvement in the properties is mainly ascribed to the contribution of SiC particles, and the strength degradation is due to the residual tensile stresses in the matrix.

Acknowledgments

This work was supported by the National Outstanding Young Scientist Foundation for Y.C. Zhou under Grant No. 59925208, Natural Sciences Foundation of China under

Grant No. 50232040, No. 50302011, No. 90403027, '863' project, ''Hundred-Talent Plan'' and High-tech Bureau of the Chinese Academy of Sciences.

References

[1] Y.C. Zhou, Z.M. Sun, Microstructure and mechanism of damage tolerance for Ti_3SiC_2 bulk ceramics, Mater. Res. Innovat. 2 (1999) 360–363.
[2] X.H. Tong, T. Okano, T. Iseki, T. Yano, Synthesis and high temperature mechanical properties of Ti_3SiC_2/SiC composite, J. Mater. Sci. 30 (1995) 3087–3090.
[3] N.F. Gao, Y. Miyamoto, D. Zhang, Dense Ti_3SiC_2 prepared by reactive HIP, J. Mater. Sci. 34 (1999) 4385–4392.
[4] M.W. Barsoum, T. El-Raghy, Synthesis and characterization of a remarkable ceramic: Ti_3SiC_2, J. Am. Ceram. Soc. 79 (1996) 1953–1956.
[5] T. El-Raghy, A. Zavaliangos, M.W. Barsoum, S.R. Kalidindi, Damage mechanisms around hardness indentation in Ti_3SiC_2, J. Am. Ceram. Soc. 80 (1997) 513–516.
[6] T. El-Raghy, M.W. Barsoum, A. Zavaliangos, S.R. Kalidindi, Processing and mechanical properties of Ti_3SiC_2: II Effect of grain size and deformation temperature, J. Am. Ceram. Soc. 82 (10) (1999) 2855–2860.
[7] Y.C. Zhou, Z.M. Sun, Electronic structure and bonding properties in layered ternary carbide Ti_3SiC_2, J. Phys.: Conden. Matter. 12 (28) (2000) L457–L462.
[8] J.Y. Wang, Y.C. Zhou, Polymorphism of Ti_3SiC_2 ceramic: first-principle investigations, Phys. Rev. B 69 (2004) 144108.
[9] Z.M. Sun, Y.C. Zhou, M.S. Li, High temperature oxidation behavior of Ti_3SiC_2-based material in air, Acta Mater. 49 (20) (2001) 4347–4353.
[10] M.W. Barsoum, L.H. Ho-doc, M. Radovic, T. El-Raghy, Long time oxidation study of Ti_3SiC_2, Ti_3SiC_2/SiC and Ti_3SiC_2/TiC composites in air, J. Electrochem. Soc. 150 (4) (2003) B166–B175.
[11] S.L. Yang, Z.M. Sun, H. Hashimoto, Y.H. Park, Oxidation of Ti_3SiC_2 at 1000 degrees C in air, Oxid. Met. 59 (1/2) (2003) 155–156.
[12] G.M. Liu, M.S. Li, Y.M. Zhang, Y.C. Zhou, Oxidation behavior of silicide coating on Ti_3SiC_2-based ceramic, Mater. Res. Innovat. 6 (5/6) (2002) 226–231.
[13] J.X. Chen, Y.C. Zhou, Strengthening of Ti_3AlC_2 by incorporation of Al_2O_3, Scripta Mater. 50 (2004) 897–901.
[14] G.C. Wei, P.F. Becher, Improvements in mechanical properties in SiC by the addition of TiC particles, J. Am. Ceram. Soc. 67 (8) (1984) 571–574.
[15] H.J. Wang, Z.H. Jin, Y. Miyamoto, Effect of Al_2O_3 on mechanical properties of Ti_3SiC_2/Al_2O_3 composite, Ceram. Int. 28 (2002) 931–934.
[16] Y. Du, J.C. Schuster, H.J. Seifert, F. Aldinger, Experimental investigation and thermodynamic calculation of the titanium–silicon–carbon system, J. Am. Ceram. Soc. 83 (1) (2000) 197–203.
[17] S.B. Li, J.X. Xie, L.T. Zhang, L.F. Cheng, Mechanical properties and oxidation resistance of Ti_3SiC_2/SiC composite synthesized by in situ displacement reaction of Si and TiC, Mater. Lett. 57 (2003) 3048–3056.
[18] R. Radhakrishnan, C.H.J. Henager, J.L. Brimhall, S.B. Bhaduri, Synthesis of Ti_3SiC_2/SiC and $TiSi_2$/SiC composites using displacement reactions in the Ti–Si–C system, Scripta Mater. 34 (12) (1996) 1809–1814.
[19] L.H. Ho-Duc, T. El-Raghy, M.W. Barsoum, Synthesis and characterization of 0.3 V_f TiC–Ti_3SiC_2 and 0.3 V_f SiC–Ti_3SiC_2 composites, J. Alloys. Compd. 350 (2003) 303–312.
[20] Y.C. Zhou, H.B. Zhang, M.S. Li, J.Y. Wang, Y.W. Bao, Preparation of TiC free Ti_3SiC_2 with improved oxidation resistance by substitution of Si with Al, Mater. Res. Innovat. 8 (2) (2004) 97–102.
[21] R. Yu, L.L. He, H.Q. Ye, Effect of Si and Al on twin boundary energy of TiC, Acta Mater. 51 (2003) 2477–2484.
[22] F. Sato, J.F. Li, R. Watanabe, Reaction synthesis of Ti_3SiC_2 from mixture of elemental powders, Mater. Trans. 41 (5) (2000) 605–608.
[23] J. Lis, Y. Miyamoto, R. Pampuch, K. Tanihata, Ti_3SiC_2-based materials prepared by HIP-SHS techniques, Mater. Lett. 22 (1995) 163–168.
[24] Y.C. Zhou, Z.M. Sun, S.Q. Chen, Y. Zhang, In-situ hot pressing/solid–liquid reaction synthesis of dense titanium silicon carbide bulk ceramics, Mater. Res. Innovat. 2 (1998) 142–146.
[25] L.E. Copeland, R.H. Bragg, Quantitative X-ray diffraction analysis, Anal. Chem. 30 (2) (1958) 196–201.
[26] R.A. Young, The Rietveld Method, Oxford University press, 1993.
[27] D.B. Wiles, R.A. Young, A new computer program for Rietveld analysis of X-ray powder diffraction patterns, J. Appl. Crystallogr. 14 (1981) 149–151.
[28] R.J. Hill, C.J. Howard, Quantitative phase analysis from neturon powder diffraction data using the Rietveld Method, J. Appl. Crystallogr. 20 (1987) 467–474.
[29] Y.W. Bao, Y.C. Zhou, Evaluating high-temperature modulus and elastic recovery of Ti_3SiC_2 and Ti_3AlC_2 ceramics, Mater. Lett. 57 (2003) 4018–4022.
[30] C. Racault, F. Langlais, R. Naslain, Solid state synthesis and characterization of the ternary phase Ti_3SiC_2, J. Mater. Sci. 29 (13) (1994) 3384–3392.
[31] Y.C. Zhou, Z.M. Sun, Temperature fluctuation/hot-pressing synthesis of Ti_3SiC_2, J. Mater. Sci. 35 (17) (2000) 4343–4346.
[32] Y.C. Zhou, Z.M. Sun, B.H. Yu, Microstructure of Ti_3SiC_2 prepared by the in-situ hot processing/solid–liquid reaction process, Z. Metalkd. 91 (11) (2000) 937–941.
[33] N.P. Padture, S.J. Bennison, H.M. Chan, Flaw-tolerance and crack-resistance properties of alumina–aluminum titanate composites with tailored microstructures, J. Am. Ceram. Soc. 76 (9) (1993) 2312–2320.
[34] X.H. Wang, Y.C. Zhou, Microstructure and properties of Ti_3AlC_2 prepared by the solid–liquid reaction synthesis and simultaneous in-situ hot pressing process, Acta Mater. 50 (2002) 3141–3149.